Published in final edited form as:
Lama, S., Schmidt, J., Malik, A., Walczak, R., Varon Silva, D., Völkel, A., et al. (2018). Modification of salt-templated carbon surface chemistry for efficient oxidation of glucose with supported gold catalysts. ChemCatChem, 10(11), 2458-2465. doi:10.1002/cctc.201800104.

Modification of salt-templated carbon surface chemistry for efficient oxidation of glucose with supported gold catalysts

Sandy M. G. Lama, Johannes Schmidt, Ankita Malik, Ralf Walczak
Daniel Varon Silva, Antje Völkel, Martin Oschatz

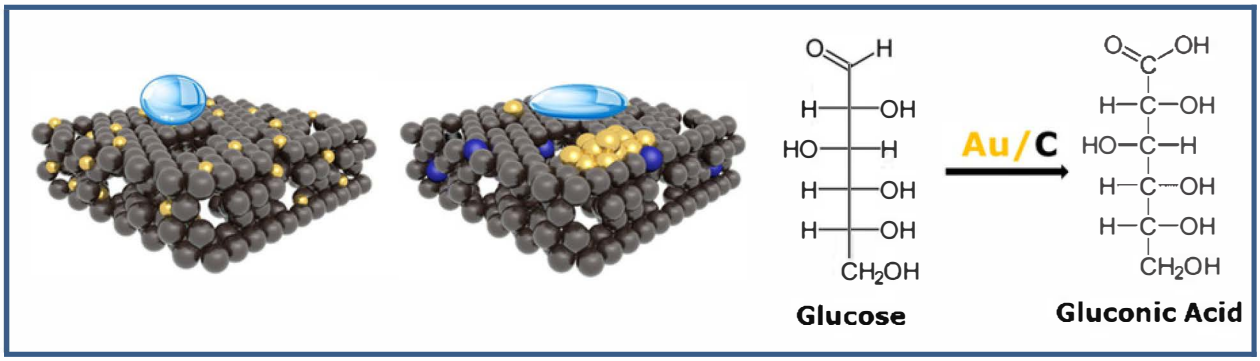

Towards the smallest gold: Salt-templated porous carbon materials are prepared and equipped with heteroatoms (H, O, or N). The surface modification influences the structural properties of gold nanoparticles catalysts deposited on the carbon surface. Smaller gold nanoparticles lead to higher catalytic activity in the selective oxidation of glucose to gluconic acid in aqueous solution.

Keywords:
heterogeneous catalysis, porous carbon, gold nanoparticles, glucose oxidation, surface polarity

Article type: Full Paper

Modification of salt-templated carbon surface chemistry for efficient oxidation of glucose with supported gold catalysts

Sandy M. G. Lama,[a] *Johannes Schmidt,*[b] *Ankita Malik,*[c] *Ralf Walczak,*[a] *Daniel Varon Silva,*[c] *Antje Völkel,*[a] *Martin Oschatz,*[a,*]

[a] Max Planck Institute of Colloids and Interfaces, Department of Colloid Chemistry, Research Campus Golm, Am Mühlenberg 1, 14476 Potsdam, Germany.

[b] Technische Universität Berlin, Institute of Chemistry, Division of Functional Materials, Hardenbergstraße 40, 10623 Berlin, Germany.

[c] Max Planck Institute of Colloids and Interfaces, Department of Biomolecular Systems, Research Campus Golm, Am Mühlenberg 1, 14476 Potsdam, Germany.

Corresponding author. Email: martin.oschatz@mpikg.mpg.de

Keywords: heterogeneous catalysis, porous carbon, gold nanoparticles, glucose oxidation, surface polarity

Abstract

Gold nanoparticles dispersed on high surface area carbon materials are investigated as heterogeneous catalysts for the selective oxidation of D-glucose to D-gluconic acid in aqueous solution with molecular oxygen. Salt-templated porous carbon supports are obtained from different precursors with and without nitrogen and treated under air or hydrogen atmosphere in order to functionalize the surface with nitrogen, oxygen, or hydrogen. The influence of the surface atomic structure of carbonaceous support materials with comparable pore structure on the size and catalytic properties of the metallic nanoparticles is studied at loadings of 0.4-0.7 wt%. These groups significantly influence the surface polarity of the support materials as well as the strength of interaction with the gold particles. This similarly influences the structure and properties of the catalysts because both the gold deposition and the glucose oxidation reaction take place in aqueous phase. Large gold particles are obtained for the rather hydrophilic supports doped with oxygen and nitrogen leading to lower catalytic activity. In contrast, the rather hydrophobic as-made and hydrogen-treated supports provide higher catalytic activity (metal time yield up to 1.5 $mol_{Glucose} \cdot mol_{Au}^{-1} \cdot s^{-1}$) resulting from their smaller gold particles of 3-5 nm in diameter.

1. Introduction

Nanostructured carbons or carbonaceous materials play an ever increasing role in heterogeneous catalysis.[1-5] On the one hand, such materials can provide intrinsic catalytic activity and thus enable metal-free catalysis, i.e. substrates that were usually believed to be activated only by "classical" metallic surfaces can also react

on carbon surfaces – especially if they are doped with heteroatoms such as nitrogen, oxygen, boron, phosphorus, sulfur, or combinations of them.[6-12] Due to the high electric conductivity of such metal-free catalysts, this possibility is of particular importance in the field of electrocatalysis.[13] On the other hand and from a more traditional perspective, nanocarbons can act as stabilizing agents (so called "supports") for catalytically active sites (in most cases metallic or other inorganic nanoparticles).[14-16] Such materials are attractive catalyst supports because of their high chemical and thermal stability as well as their weak chemical interaction with the metal particles facilitating the formation of active species.[17-18] Nanocarbons can provide high specific surface area and pore volume to disperse and stabilize the catalytically active particles.[19-20] Furthermore, their textural properties such as pore size, pore connectivity and pore geometry can be tailored over a wide range and this in turn allows additional control over size and size distribution of nanoparticles.[4] Probably even more important, carbon nanomaterials are widely tuneable in terms of their atomic architecture. Their surface and electronic properties can be influenced by the presence of heteroatoms and/or surface functional groups.[5, 21] Such structure motives can not only lead to intrinsic catalytic effects but also have strong effects on the metals involved in the catalytic process.[3, 22-24] Furthermore, the surface chemical properties of carbon materials (in combination with the pore and particle structure) will be crucial for the interaction of the catalyst with the surrounding phases. A metal particle deposited on a carbon support will likely be more prone towards oxidation if it is surrounded by a large number of oxygen-containing surface functional groups such as hydroxyls, ketones, or carboxyls. Moreover, surface functional groups can enhance the

interaction with the metal particles and therefore serve as so called "anchoring points" which can slow down particle growth.[21] While these are widely known and studied effects of heteroatoms in carbon supports on metallic nanoparticles, the influence of such functional groups are less investigated with regard to the interaction with the surrounding phase, which is of particular importance for catalytic reactions and catalyst synthesis in liquid phase. In many cases, the interference with other crucial structural parameters such as particle size, active material loading, and porosity is the particular problem for drawing accurate conclusions on the influence of surface functionalities of the carbon supports on the catalytic properties.

To investigate the interplay between carbon surface structure and catalytic properties, we deposited pre-reduced and citrate-stabilized gold nanoparticles on porous salt-templated carbon support materials derived from glucose ($C_{Glucose}$) with hierarchical pore structure containing micro- and mesopores. Prior to gold deposition, the surface structure of the as-made $C_{Glucose}$ has been modified with a higher density of oxygen-containing surface groups ($C_{Glucose}$-O) by treatment under air atmosphere or large parts of the oxygen surface groups have been replaced under hydrogen atmosphere at high temperature ($C_{Glucose}$-H). Furthermore, a nitrogen-doped sample ($C_{Glucosamine}$)[14] with comparable porosity to $C_{Glucose}$ was prepared by using glucosamine instead of glucose as the carbon precursor.

In order to investigate the influence of the different support materials on the structures of the catalysts and on the catalytic properties of the gold nanoparticles (AuNPs), the Au-C catalysts were applied in the oxidation of D-glucose to D-gluconic acid in aqueous solution with molecular oxygen as the oxidizing agent.

This conversion is a widely applied model reaction for the investigation of supported gold catalysts in liquid phase[25-29] but it is also of commercial relevance because the annual production of gluconic acid amounts to ~100000 t.[30] It is used as a functional additive in food, pharmaceutical products, and textiles but also in building industries. It is currently mainly produced by biotechnological processes (fermentation).[30-32] However, gold nanoparticles are a promising alternative for the production of gluconic acid at comparable reaction rate and high space time yield.[33] From a mechanistical point of view is widely accepted that the gluconic acid is produced together with hydrogen peroxide. The latter decomposes immediately in the alkaline reaction medium. Furthermore, it has been proposed that the catalytic conversion proceeds via an Eley–Rideal mechanism. A glucose molecule is adsorbed on the catalyst and converted by an oxygen molecule from the liquid phase.[33] Nanostructured carbon materials are a particularly attractive support for AuNPs in this reaction as compared to oxidic supports due to higher turnover frequency and catalytic activity.[34] In general the catalytic activity is strongly dependent on the gold particle size and shows a sharp increase if the diameter of the AuNPs falls below 5 nm. Multiple studies on the influence of catalyst synthesis (i.e., gold deposition) methods,[35] textural properties of supports,[36-37] and reaction conditions[38] on the properties of supported gold catalysts in the oxidation of glucose to gluconic acid exist but the influence of the presence of heteroatoms/surface functional groups on the structure of the catalysts and the resulting catalytic properties is only rarely investigated.[36] We find a significant influence of the surface chemistry of the salt-templated carbon support materials derived from glucose on the structural properties of the resulting catalysts and thus

also on the catalytic performance (**Scheme 1**). Supports with rather polar/hydrophilic surface structure ($C_{Glucose}$-O and $C_{Glucosamine}$) have much larger gold particles after deposition from aqueous solution and thus a lower catalytic activity as compared to supports with less polar surface ($C_{Glucose}$-H and $C_{Glucose}$-O).

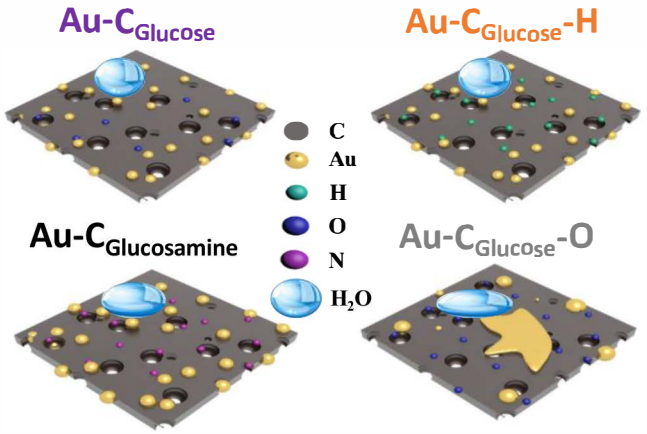

Scheme 1. Structure of gold catalysts on salt-templated porous carbon supports with different surface polarity.

2. Results and discussion

2.1. Structural characterization of the catalysts and the supports

Four different catalyst supports were used in order to study the effects of the carbon surface chemistry on the properties of the resulting Au-C catalysts. The $C_{Glucose}$ carbon and the N-doped $C_{Glucosamine}$ carbon were prepared from different precursors. $C_{Glucose}$-H and $C_{Glucose}$-O were prepared by treatment of $C_{Glucose}$ under hydrogen and air atmosphere, respectively.

Elemental analyses (EA) of the supports (**Table 1**) show that $C_{Glucose}$-O has significantly higher oxygen content as compared to the as-made $C_{Glucose}$ showing that the treatment under air at 400 °C does indeed introduce more oxygen-

containing functional groups on the surface of the carbon material. The treatment under reductive atmosphere does only slightly reduce the oxygen content of the carbon. However, it should generally be kept in mind that such measurements are influenced by molecules (e.g., water or carbon dioxide) adsorbed in the narrow pores of the support materials. This explains the significant oxygen content detected in $C_{Glucose}$-H and also in $C_{Glucose}$. In agreement with a previous study,[14] the use of Glucosamine as precursor leads to a nitrogen content of 2.6 wt%. No significant amounts of nitrogen have been detected in the other supports. The presence of nitrogen into the carbon framework or nitrogen-containing surface groups in $C_{Glucosamine}$ is further proven by XPS measurements of the Au-C catalysts (**Table 2**). The oxygen content of $C_{Glucosamine}$ is also much higher than in $C_{Glucose}$. This might again result from the higher surface polarity and thus larger amount of water adsorbed in this material. Similar trends in terms of elemental composition are detected for the carbon materials after gold deposition indicating that the functionalization with AuNPs in liquid phase has no major influence on the heteroatom content of the supports.

Further insights into the different surface structures of the Au-C catalysts are obtained by TGA analysis after deposition of AuNPs (Supporting Information, **Figure S1**). Au-$C_{Glucose}$-H shows the smallest weight loss resulting from removal of the oxygen-containing surface groups present in as-made $C_{Glucose}$. In accordance to their lower carbon content detected in EA, Au-$C_{Glucose}$-O and Au-$C_{Glucosamine}$ have a higher number of thermally decomposable surface groups and thus show a higher weight loss up to 800°C. The significant mass loss up to temperatures of 100°C and slightly above indicates the potential presence of water adsorbed on the

catalysts – especially in Au- $C_{Glucose}$-O and Au-$C_{Glucosamine}$ this is in line with the EA results discussed above and also with the water vapor adsorption measurements discussed below.

Table 1. Porosity and elemental analysis data summary of the support materials and the Au-C catalysts.

Support/Catalyst	SSA ($m^2 \cdot g^{-1}$)	TPV ($cm^3 \cdot g^{-1}$)	MPV ($cm^3 \cdot g^{-1}$)	C/N/H/O $(wt\%)_{EA}$
$C_{Glucose}$	705	0.62	0.18	85.6/0.2/1.3/11.9
$C_{Glucose}$-O	1032	1.10	0.28	70.8/0.2/1.7/26.4
$C_{Glucose}$-H	904	0.93	0.25	87.3/0.2/1.3/10.2
$C_{Glucosamine}$	807	1.26	0.16	72.7/2.6/1.7/21.9
Au-$C_{Glucose}$	559	0.98	0.09	88.7/0.4/1.4/9.4
Au-$C_{Glucose}$-O	926	0.78	0.28	75.6/0.2/2.0/22.3
Au-$C_{Glucose}$-H	935	1.02	0.26	92.8/0.3/2.1/4.7
Au-$C_{Glucosamine}$	812	1.22	0.16	75.9/2.7/1.7/19.8

All supports show nitrogen physisorption isotherms with a high nitrogen uptake at low relative pressure and a hysteresis loop in the range of $P \cdot P_o^{-1} > 0.8$ (**Figure 1A**). Accordingly, the QSDFT analysis of the isotherms shows a broad pore size distribution including micropores and mesopores of different sizes (**Figure 1C**). The salt-templated carbons have SSAs in the range of 700-1000 $m^2 \cdot g^{-1}$ and TPVs (up to 50 nm) of 0.6-1.26 $cm^3 \cdot g^{-1}$ (**Table 1**). The $C_{Glucose}$ support shows a slightly lower porosity as compared to the other carbons. Especially $C_{Glucosamine}$ contains a larger volume of 10-30 nm sized mesopores. The micropore volumes of after-

treated $C_{Glucose}$-O (0.28 $cm^3 \cdot g^{-1}$) and $C_{Glucose}$-H (0.25 $cm^3 \cdot g^{-1}$) are slightly higher as compared to as-made $C_{Glucose}$ (0.18 $cm^3 \cdot g^{-1}$) and $C_{Glucosamine}$ (0.16 $cm^3 \cdot g^{-1}$).

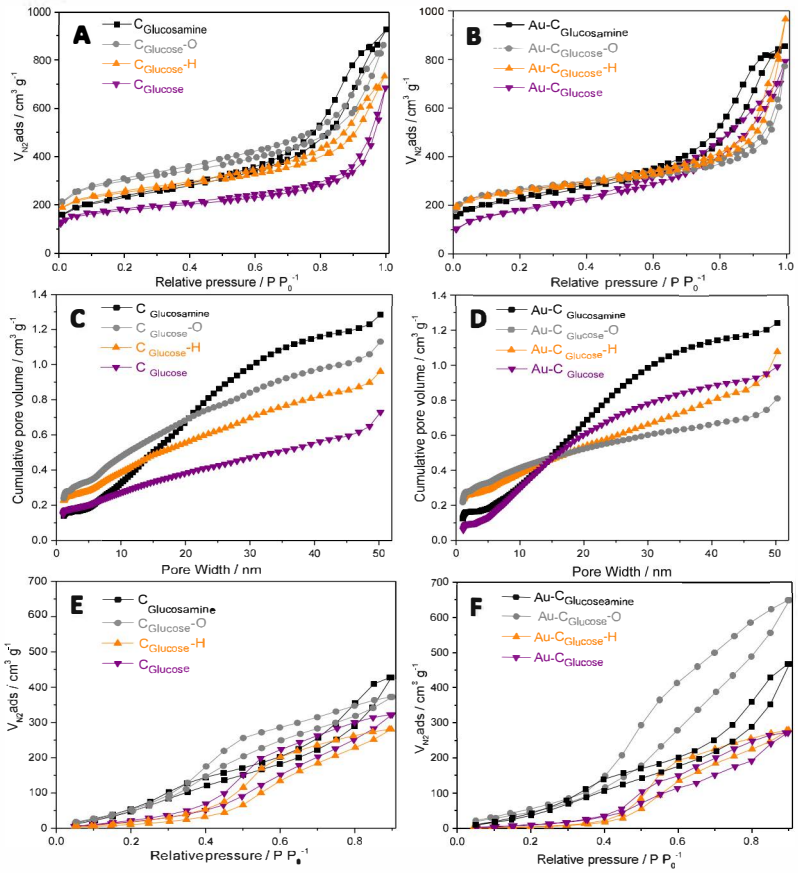

Figure 1. Nitrogen physisorption isotherms (A,B) with corresponding cumulative pore size distributions (C,D) and water vapor physisorption isotherms (E,F) of the pristine catalyst supports (A,C,E) as well as the Au-C catalysts (B,D,F).

Despite these minor differences, the general pore structure of the supports remains comparable even after the substitution of glucose with glucosamine and the post-synthesis treatments under air and hydrogen. TEM images of the as-made carbon supports (**Figure S2**) show an open mesopore system with comparable structure in the materials independent of the surface chemistry. After deposition of the AuNPs, nitrogen physisorption isotherms do not significantly change in shape indicating that the general mesopore structure of the carbons remains unaffected by the

presence of metal nanoparticles. Interestingly, the decrease of the micropore volume in comparison to the pristine support is most distinctive for Au-$C_{Glucose}$. This indicates that more small pores must be clogged by small particles in this catalyst.

In addition to changes of the atomic structure of the carbon surface, the modification of the support materials with surface functional groups and heteroatoms will significantly influence the interaction with water, that is, the surface hydrophilicity /hydrophobicity. This is of particular importance for catalytic reactions and catalyst synthesis in aqueous phases. Water vapor adsorption isotherms of the catalyst supports at 25 °C (**Figure 1E**) show that the $C_{Glucosamine}$ and $C_{Glucose}$-O supports are more hydrophilic than $C_{Glucose}$-H and $C_{Glucose}$, because the onset of water adsorption (a standard indicator for the strength of interaction of water with surfaces) is located at smaller relative pressure. The strength of the interaction of water vapor with the carbon surface is mainly dominated by the carbon pore size and the density of surface functional groups in the carbon framework that can lead to specific interactions with the adsorbate.[39] Taking the comparable pore size distribution of the supports into consideration, the lower pressure needed to bind water to the support surface shows the more hydrophilic properties of $C_{Glucosamine}$ and $C_{Glucose}$-O. After loading of the AuNPs, this trend between the samples can still be observed (**Figure 1F**). Whereas the isotherms of Au-$C_{Glucosamine}$ and Au-$C_{Glucose}$-H, and Au-$C_{Glucose}$ remain comparable in shape and water uptake to the pristine supports, Au-$C_{Glucose}$-O shows a more distinct uptake at 0.5-0.9 $P \cdot P_o^{-1}$. This indicates that the surface of this sample becomes more attractive for water adsorption after deposition of the metal. Despite

of the generally more hydrophobic surface properties of carbon in comparison to oxidic catalyst support materials, the surface wetting and dispersability in water of the salt-templated carbon supports discussed here is sufficient for both catalyst synthesis and catalytic reaction in aqueous solution. In contrast to the surface polarity, the microstructure of the carbon framework shows no significant changes after the different functionalization treatments and gold deposition. Raman spectroscopy measurements of the Au-C catalysts show the typical appearence for disordered amorphous carbon materials with the D- and G-band at ~ 1340 cm^{-1} and 1580 cm^{-1}, respectively (**Figure S3**). The comparable I_D/I_G values which are widely employed to estimate the degree of carbon ordering in such materials, remains comparable in all catalysts (1.03-1.13).

TEM measurements of the Au-C catalysts (**Figure 2, Figure S4** and **Table 2**) show the presence of small and well-distributed AuNPs on the surface of $C_{Glucose}$-H and $C_{Glucose}$, that is, on the supports with rather hydrophobic surface properties. The Au-$C_{Glucose}$ catalyst contains slightly smaller AuNPs with more narrow distribution (3.4 ± 1.1 nm) as compared to Au-$C_{Glucose}$-H (4.4 ± 2.4 nm). The size of AuNPs in these two catalysts is in the same range as compared to the AuNPs in the original colloidal solution which was determined to be 4.05 ± 1.05 nm by TEM after water evaporation (**Figure S5**). In contrast, larger gold particles are present on Au-$C_{Glucosamine}$ (6.8 ± 2.4 nm) and Au-$C_{Glucose}$-O with more hydrophilic surface properties. Especially the Au-$C_{Glucose}$-O catalyst contains additionally very large gold particles and only a minor fraction of the metal is present as particles with sizes below 10 nm (**Figure S4**).

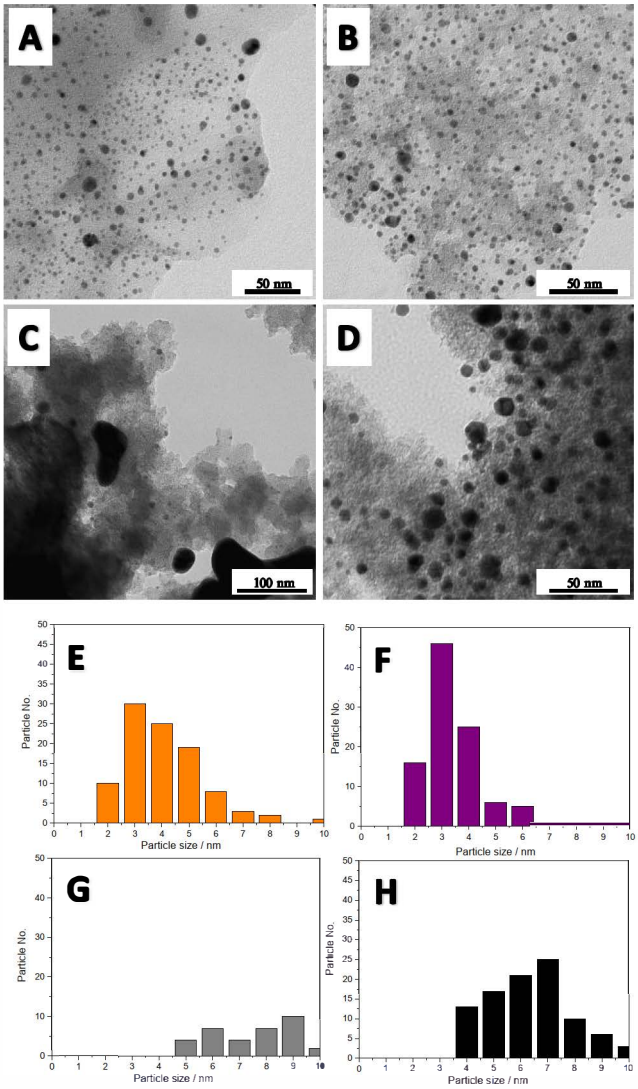

Figure 2. TEM images (A-D) and corresponding AuNP size distributions up to 10 nm (E-H) of Au-$C_{Glucose}$-H (A,E), Au-$C_{Glucose}$ (B,F), Au-$C_{Glucose}$-O (C,G), and Au-$C_{Glucosamine}$ (D,H).

It can be concluded that enhanced surface wetting of carbons with more polar/hydrophilic surface leads to different kinetics of ligand exchange around the AuNPs from the citrate stabilizer to the carbon support. The resulting differences in the rate of AuNP deposition most likely result in coalescence of AuNPs and thus larger particles on the surface of the rather hydrophilic carbon supports after deposition.

Table 2. XPS and ICP data summary, average particle sizes before and after (given in brackets) glucose oxidation reaction, and gold-specific activity (expressed as metal time yield, MTY) of the Au-C catalysts.

Catalyst	C/N/O/Au $(atom\%)_{XPS}$	Au $(wt\%)_{ICP}$	Average Au size $(nm)_{TEM}$	MTY $(mol_{Glucose} \cdot mol^{-1}_{Au} \cdot s^{-1})$
Au-$C_{Glucose}$	90/-/6.7/2.7	0.4	3.4 ± 1.1 (3.8±1.2)	1.5
Au-$C_{Glucose}$-O	89/-/10/0.5	0.4	n. d.	n. d.
Au-$C_{Glucose}$-H	90/-/9.9/0.4	0.4	4.4 ± 2.4 (5.2±2.5)	1.0
Au-$C_{Glucosamine}$	88/1.8/8.6/1.3	0.7	6.8 ± 2.4 (8.4±3.8)	0.2

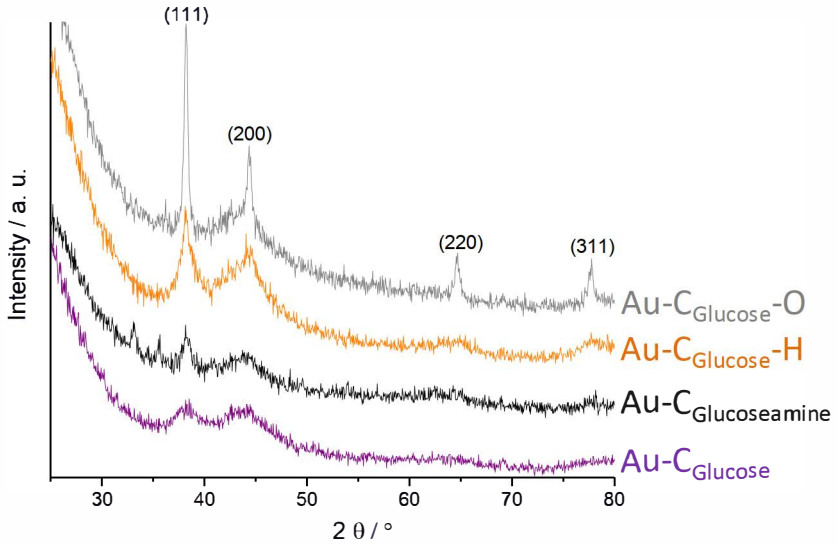

Figure 3. XRD patterns of the Au-$C_{Glucose}$, Au-$C_{Glucose}$ -H, Au-$C_{Glucosamine}$, and Au-$C_{Glucose}$-O catalysts.

In agreement with the TEM images, the XRD pattern of the calcined Au-$C_{Glucose}$-O catalyst shows comparably sharp peaks originating from chunks of elemental gold on the surface of the carbon support. In contrast, significantly broadened peaks in

XRD patterns of the other Au-C catalysts are caused by the very small nanoparticles present in these catalysts (**Figure 3**).

The gold content in the catalysts was determined with ICP-OES is 0.4 wt% (**Table 2**). Au-$C_{Glucosamine}$ shows a higher gold loading of 0.7 wt% due to the larger amount of adsorbed water in the support prior to AuNP deposition. The relatively high error of the ICP-OES measurements at such low metal loadings can be another reason for the differences in gold loading between the samples. XPS measurements of the Au-C catalysts (averaged data from multiple measurements on different spots of the particles) show that the gold content on the particle surface is 0.4-2.7 atom% (**Table 2** and **Figure S6**). Compared with the much lower bulk Au content determined with ICP-OES this indicates that the metal particles are mainly located at the external surfaces of the support particles, i.e., they are not entering the entire internal porosity during deposition from aqueous solution. Scans of the Au4f peaks (**Figure S7**) of all catalysts show comparable shape for all catalysts. The typical doublet signal for metallic gold is present at binding energies of ~84.0 and ~87.5 eV in accordance to the XRD measurements and no significant contribution of oxidized gold species is detected.

From the structural characterization of the catalysts it can be concluded that the presence of different surface chemistries leads to significant differences in the structures after synthesis and that catalytic properties will be mainly affected by variations in the gold particle size and surface properties of the supports at otherwise comparable support porosity and reduction state of the gold.

2.2. Catalytic properties in glucose oxidation

The freshly synthesized Au-C catalysts are applied for glucose oxidation reaction at pH = 9, 45°C, and with an air flow of 250 $mL \cdot min^{-1}$ while stirring with a magnetic stirrer at 800 rpm. The glucose solution is prepared as 0.1 M in distilled water, where only 50 mL of 0.1 M aqueous glucose is used for each reaction and the pH changes are adjusted with 1 M aqueous NaOH solution during conversion of glucose to gluconic acid.

Tiration curves show that all catalysts but Au- $C_{Glucose}$-O reach the maximum conversion but at different specific activity (**Figure 3A** and **Table 2**), which is in the following expressed as metal time yield given in $mol_{Glucose} \cdot mol^{-1}_{Au} \cdot s^{-1}$. Au-$C_{Glucose}$ (1.5 $mol_{Glucose} \cdot mol^{-1}_{Au} \cdot s^{-1}$) and Au-$C_{Glucose}$-H (1.0 $mol_{Glucose} \cdot mol^{-1}_{Au} \cdot s^{-1}$) show the highest MTYs of all catalysts studied. They have a rather hydrophobic surface chemistry as it has been seen in water vapour physisorption measurements (**Figure 1F**) in combination with very small AuNPs which is of particular importance to achieve rapid glucose conversion. In contrast, Au-$C_{Glucose}$-O (no notable conversion) and Au-$C_{Glucosamine}$ (0.2 $mol_{Glucose} \cdot mol^{-1}_{Au} \cdot s^{-1}$) have significantly lower catalytic activity, presumably due to the much larger gold particles in comparison to the rather hydrophobic supports. Another reason for the lower activity of these two catalysts could be the stronger adsorption of the substrate and product molecules in the reaction solution with the porous catalyst support and thus slower transport to the catalytically active centers.

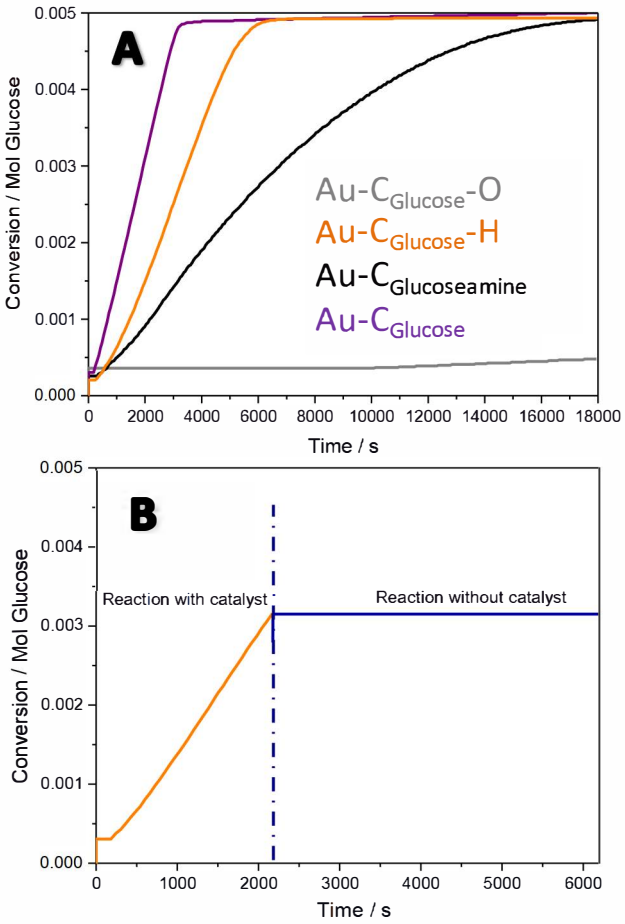

Figure 4. Glucose conversion of the Au-$C_{Glucose}$, Au-$C_{Glucose}$-H, Au-$C_{Glucosamine}$, and Au-$C_{Glucose}$-O catalysts as a function of time (A) and heterogeneity test of Au-$C_{Glucose}$-H (B). Reaction conditions: ϑ = 45°C, pH = 9, O_2 flow ~ 250 mL·min^{-1}, $C_{Glucose}$ = 0.1 mol·L^{-1}, V = 50 mL, magnetic stirring at 800 rpm.

After reaction, the catalysts are separated from the solution via centrifugation and the gluconic acid selectivity is analysed by HPLC analysis of the liquid phase. According to the HPLC analysis results all the catalysts are selective to gluconic acid formation under the elevated conditions and all except Au-$C_{Glucose}$-O achieve full conversion of glucose which is in line with the results of the titration experiments (**Figure S8**).

As gluconic acid is applied in pharmaceuticals and food additives,[30] it is important for safety and health matters not to have any Au nanoparticles leaking in the product of the glucose conversion. Therefore, a heterogeneity test is performed exemplarily for the Au-$C_{Glucose}$-H catalyst to check for loss of Au nanoparticles from the support. The reaction is started and titrated under the standard conditions. After a certain time, the catalyst is filtered from the solution and the reaction is continued without the Au-C (**Figure 4B**). The result shows that the reaction is stopped completely after filtration of the catalyst, meaning that no Au nanoparticles are leaking in the solution and only carbon-supported AuNPs are active for oxidation of glucose.

The catalysts are washed twice with distilled water then dried at 60 °C overnight. Finally, the particle size of the spent catalysts was analysed with TEM. Only few small AuNPs are present in Au-$C_{Glucose}$-O after reaction in accordance to XRD and TEM investigations of the fresh catalyst. Although all other catalysts have been active in glucose conversion and achieved full conversion under the elevated conditions, the AuNPs are only a bit larger in size compared to the fresh catalysts (**Table 2**) and well dispersed over the support surface (**Figure 5**). AuNPs of Au-$C_{Glucosamine}$ showed the most distinctive growth during the first catalytic cycle which is in line with recyclability tests (**Figure S9**). The average diameter AuNPs of the Au-$C_{Glucosamine}$ increased from 6.8 to 8.4 nm and thus there is a notable loss of catalytic activity in the second cycle. In contrast, the titration curves of Au-$C_{Glucose}$-H and Au-$C_{Glucose}$ show nearly unchanged catalytic activity during the second cycle.

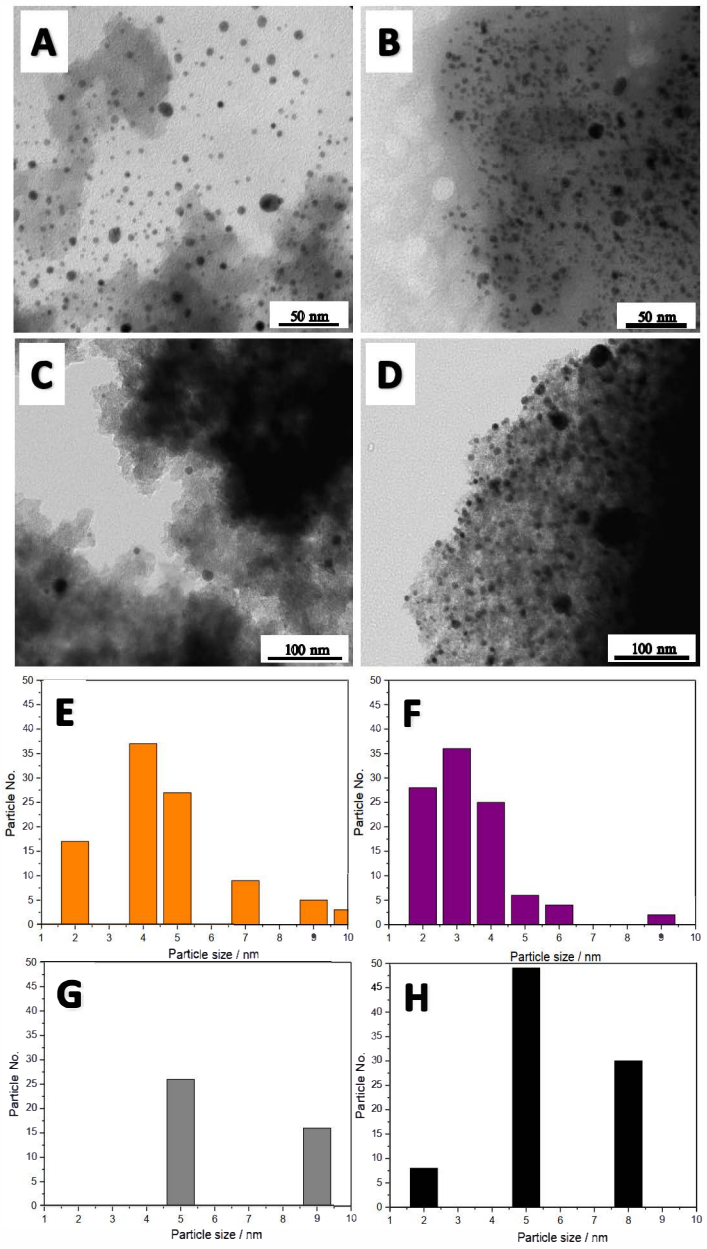

Figure 5. TEM images (A-D) and corresponding AuNP size distributions up to 10 nm (E-H) of the spent catalysts Au-$C_{Glucose}$-H (A,E), Au-$C_{Glucose}$ (B,F), Au-$C_{Glucose}$-O (C,G), and Au-$C_{Glucosamine}$ (D,H).

3. Conclusions

The surfaces of salt-templated porous carbon materials with comparable pore structure have been equipped with different heteroatoms (H, O, and N) and their influence on the structural properties of gold nanoparticles deposited on their

surface has been investigated. Non-polar carbon surfaces lead to smaller gold particles and thus higher catalytic activity in selective oxidation of glucose to gluconic acid in aqueous solution at 45 °C and pH = 9 with molecular oxygen as oxygen source. Au-$C_{Glucose}$, Au-$C_{Glucose}$-H, and Au-$C_{Glucosamine}$ reached full and selective conversion but the latter catalyst showed lower activity resulting from larger gold particles. Au-$C_{Glucose}$-O showed no glucose conversion due to the strong agglomeration of the gold particles during deposition on the hydrophilic support.

Hence, it can be concluded that the surface structure of the carbon materials has a significant direct influence on the deposition mechanism of gold from aqueous solution and on the structure of the catalysts. This results in an indirect influence of the support surface structure on the catalytic activity in the oxidation of glucose in aqueous phase at unchanged selectivity. In contrast, a significant influence of the surface properties of the carbon materials as such on the catalytic reaction has not become apparent in this study due to the strong effect of the different sizes of AuNPs on the catalytic activity. Since only minor apparent changes of the carbon surface chemistry give such a significant difference in the structures of the catalysts, there is a huge importance of precisely adjusting this property of the carbons for the synthesis of suitable heterogeneous catalysts for liquid phase reactions. Since in most of these reactions there is a strong dependency of catalytic activity on the size of AuNPs, these findings can be seen as being generally applicable for the synthesis of carbon-supported gold catalysts also for other reactions such as oxidation of cycloalkanes, alkenes or other alcohols.[24, 40-41]

4. Experimental

4.1. Synthesis of carbon supports

The porous carbon supports were prepared by salt-melt templating followed by carbonization as described previously.[14] 450 mg of an eutectic salt mixture of KCl and $ZnCl_2$ (1:2 mass ratio) was mixed with 150 g of glucose (or glucosamine) as the carbon precursor in a mortar. The mixture was heated up to 900 °C for 1 h under nitrogen atmosphere with a ramp of 2.5 $K \cdot min^{-1}$. After carbonization and cooling to room temperature, the carbon is grinded and washed with deionized water to remove possible remaining salts. Finally, the carbon was dried for 48 h at 60 °C. Instead of glucose, glucosamine hydrochloride was used as precursor for the synthesis of $C_{Glucosamine}$ with nitrogen-doping. Glucose was used for synthesis of the nitrogen-free $C_{Glucose}$ support.

For the synthesis of $C_{Glucose}$-H, part of the $C_{Glucose}$ was treated at 600°C under a flow of 5% H_2 in Ar at 600 °C for 2 h. $C_{Glucose}$-O was synthesized by heating $C_{Glucose}$ under air at 400 °C for 1 h.

4.2. Synthesis of gold on carbon catalysts

The deposition of AuNPs on carbon supports was done by first synthesizing reduced colloidal gold nanoparticles. AuNPs were prepared by mixing 500 mL of water and 29 mL of 0.2 wt% $HAuCl_4 \cdot 3H_2O$ (49 wt% Au) while stirring. Then 11.6 mL of a solution of 1 wt% sodium citrate in water was added. After 30 s, 5.80 mL of sodium borohydride mixture (85 mg of $NaBH_4$ in 50 mL of ice-cooled 1 wt% sodium citrate solution in water) was added to reduce the AuNPs.

In order to deposit the pre-reduced AuNPs on the different carbon materials, the supports were immersed into a defined volume of the nanoparticle solution under sonication in a vial for 2 h. The color of the wine-red solution turned to transparent, and the Au-loaded samples were separated by centrifugation at 4000 rpm for 20 min. Finally, the samples were dried overnight in a vacuum oven at 80 °C.

4.3. Characterization of support materials and Au-C catalysts

Transmission electron microscopy (TEM) images were obtained by using a Zeiss EM 912Ω TEM microscope at an acceleration voltage of 120 kV. The samples were dropwise immobilized on the carbon-coated copper TEM grid after dispersing in ethanol. The Particle size distributions were calculated manually using the Image J software (v. 1.47). High-angle annular dark field scanning transmission electron microscopy (HAADF-STEM) images of the pristine AuNPs after evaporation were obtained on a double-corrected Jeol ARM200F microscope equipped with a cold field emission gun utilizing a Gatan GIF Quantum. The acceleration voltage was 200kV.

Nitrogen physisorption experiments were carried out at -196 °C at a Quantachrome Quadrasorb apparatus. Before starting the analysis samples were degassed at 150 °C for 20 h. Results were analysed with the QuadraWin software (version 5.05). Pore size distributions (PSDs), specific surface areas (SSAs), total pore volumes (TPVs) up to 50 nm, and micropore volumes (MPVs) were calculated from isotherm analysis with the quenched solid density functional theory (QSDFT) method for nitrogen adsorbed on carbon with slit/cylindrical/spherical pores at -196 °C (adsorption branch kernel).

Water vapour physisorption isotherms were measured with a Quantachrome Autosorb IQ instrument at 25 °C.

The Elemental analysis was carried out by combustion analysis in a Vario Micro device.

X-ray photoelectron spectroscopy (XPS) measurements were performed using a Thermo Scientific K-Alpha+ X-ray Photoelectron Spectrometer. All samples were analyzed using a microfocused, monochromated Al Kα X-ray source (1486.68 eV; 400 μm spot size). The K-Alpha+ charge compensation system was employed during analysis to prevent any localized charge buildup. The samples were mounted on conductive carbon tape and each sample was measured at 10 different spots. The spectra of the 10 spots were averaged and the resulting spectra analyzed using the Avantage software from Thermo Scientific.

Thermogravimetric analyses (TGA) were performed using a thermo microbalance TG 209 F1 Libra from Netzsch. A platinum crucible was used for the measurement of 10 ± 1 mg of samples in a nitrogen flow of 20 $ml \cdot min^{-1}$ and a purge flow of 20 $ml \cdot min^{-1}$. The samples were heated with to 800 °C with 2.5 $K \cdot min^{-1}$.

X-ray diffraction (XRD) experiments were carried out with a Bruker D8 diffractometer and with a CuKα source (λ = 0.154 nm) and a Scintillation counter. The reference patterns were found in the ICDD PDF-4+ database (2014 edition).

Raman spectroscopy measurements were performed using a Renishaw inVia Raman Microscope operating with an objective (Nikon, 10x/0.25, ∞/− WD 6.1) and an excitation wavelength of 532 nm with a laser power of 4.0 mW. The D, D^2, A, and G bands were fitted with a Lorentz function.

Inductively coupled plasma-optical emission spectrometry (ICP-OES) was conducted using a Horiba Ultra 2 instrument equipped with photomultiplier tube detection. Prior to the measurements the carbon supports were burned off at 800 °C under air atmosphere in a muffle furnace and the residual material was dissolved in aqua regia prior to the measurements.

4.4. Catalytic testing in glucose oxidation

The oxidation reaction of D-glucose to D-gluconic acid was carried out with a 50 mL solution of 0.1 M D-glucose in deionized water at 45 °C, pH = 9, and under an oxygen flow of ~250 mL.min^{-1}. After heating to 45 °C and saturation of the solution with oxygen for ~30 min, the catalysts were added while the gas flow and temperature remained constant. The pH of the solution was kept constant at pH = 9 by automatic titration of 1 M aqueous NaOH solution with a TitroLine® 6000/7000 device. The conversion of D-glucose to D-gluconic acid was investigated for 300 min for each catalyst. The reaction mixture was constantly stirred with a magnetic stirrer at 800 rpm. The catalytic activity was directly evaluated from the titration curve. It is expressed as metal time yield (MTY) in moles of converted glucose per mole of gold per second and calculated from the average slope of the titration curve between 20 and 80 % glucose conversion.

The heterogeneity test was carried out by filtering the reaction solution before achieving complete conversion in order to remove the catalyst. Then, the filtered solution was returned to the flask and the reaction was started again with the same conditions as before filtration.

Recyclability tests of the catalysts were carried out by decanting the converted glucose solution after a first run and subsequent continuation of the titration by adding a fresh and pre-heated glucose solution.

The products of the D-glucose oxidation reaction were analysed using high performance liquid chromatography (HPLC) with an Agilent 1200 spectrometer. The products were separated over a Hypercarb column (150 x 4.6 mm) at a flow rate of 0.7 mL H_2O with 0.1 % formic acid as eluents (5 min isocratic, then a linear gradient to 20% acetonitrile (ACN) for 15 min, followed by a linear gradient to 100% ACN for 5 min.

Author Contributions

The manuscript was written through contributions of all authors. All authors have given approval to the final version of the manuscript.

Supporting Information

For further details about the experimental methods and characterization of the materials refer to the given Supporting Information.

Acknowledgment

Financial support by the Max Planck Society is gratefully acknowledged. We also thank Ms. Jeanette Steffen (Max Planck Institute of Colloids and Interfaces, Biomaterials Department) for her help with the ICP-OES measurements and Mr. Runyu Yan (Max Planck Institute of Colloids and Interfaces, Colloid Chemistry Department) for his help with the graphics.

References

[1] J. Zhu, A. Holmen, D. Chen, *ChemCatChem*, **2013**, *5*, 378-401.

[2] Y. Zhai, Z. Zhu, S. Dong, *ChemCatChem*, **2015**, *7*, 2806-2815.

[3] X. H. Li, M. Antonietti, *Chem. Soc. Rev.*, **2013**, *42*, 6593-6604.

[4] D. S. Su, S. Perathoner, G. Centi, *Chem. Rev.*, **2013**, *113*, 5782-5816.

[5] F. Rodriguez-Reinoso, *Carbon*, **1998**, *36*, 159-175.

[6] D. Yu, E. Nagelli, F. Du, L. Dai, *J. Phys. Chem. Lett.*, **2010**, *1*, 2165-2173.

[7] D. S. Su, J. Zhang, B. Frank, A. Thomas, X. Wang, J. Paraknowitsch, R. Schlogl, *ChemSusChem*, **2010**, *3*, 169-180.

[8] L. Yang, S. Jiang, Y. Zhao, L. Zhu, S. Chen, X. Wang, Q. Wu, J. Ma, Y. Ma, Z. Hu, *Angew. Chem. Int. Ed.*, **2011**, *50*, 7132-7135.

[9] Y. Zheng, Y. Jiao, L. Ge, M. Jaroniec, S. Z. Qiao, *Angew. Chem. Int. Ed.*, **2013**, *52*, 3110-3116

[10] D. S. Yang, D. Bhattacharjya, S. Inamdar, J. Park, J. S. Yu, *J. Am. Chem. Soc.*, **2012**, *134*, 16127-16130.

[11] S. Yang, L. Zhi, K. Tang, X. Feng, J. Maier, K. Müllen, *Adv. Funct. Mater.*, **2012**, *22*, 3634-3640.

[12] X. K. Kong, C. L. Chen, Q. W. Chen, *Chem. Soc. Rev.*, **2014**, *43*, 2841-2857.

[13] P. Trogadas, T. F. Fuller, P. Strasser, *Carbon*, **2014**, *75*, 5-42.

[14] S. M. G. Lama, J. Pampel, T.-P. Fellinger, V. P. Beškoski, L. Slavković-Beškoski, M. Antonietti, V. Molinari, *ACS Sustainable Chem. Eng.*, **2017**, *5*, 2415-2420.

[15] M. Oschatz, T. W. van Deelen, J. L. Weber, W. S. Lamme, G. Wang, B. Goderis, O. Verkinderen, A. I. Dugulan, K. P. de Jong, *Catal. Sci. Technol.*, **2016**, *6*, 8464-8473.

[16] L. Borchardt, F. Hasché, M. R. Lohe, M. Oschatz, F. Schmidt, E. Kockrick, C. Ziegler, T. Lescouet, A. Bachmatiuk, B. Büchner, D. Farrusseng, P. Strasser, S. Kaskel, *Carbon*, **2012**, *50*, 1861-1870.

[17] H. M. Torres Galvis, J. H. Bitter, C. B. Khare, M. Ruitenbeek, A. I. Dugulan, K. P. de Jong, *Science*, **2012**, *335*, 835-838.

[18] M. Oschatz, W. S. Lamme, J. Xie, A. I. Dugulan, K. P. de Jong, *ChemCatChem*, **2016**, *8*, 2846-2852.

[19] M. Li, F. Xu, H. Li, Y. Wang, *Catal. Sci. Technol.*, **2016**, *6*, 3670-3693.

[20] P. Zhang, H. Zhu, S. Dai, *ChemCatChem*, **2015**, *7*, 2788-2805.

[21] W. Xia, *Catal. Sci. Technol.*, **2016**, *6*, 630-644.

[22] L. M. Chew, W. Xia, H. Düdder, P. Weide, H. Ruland, M. Muhler, *Catal. Today*, **2016**, *270*, 85-92.

[23] M. Oschatz, J. P. Hofmann, T. W. van Deelen, W. S. Lamme, N. A. Krans, E. J. Hensen, K. P. de Jong, *ChemCatChem*, **2017**, *9*, 620-628.

[24] B. Donoeva, N. Masoud, P. E. de Jongh, *ACS Catal.*, **2017**, *7*, 4581-4591.

[25] H. Okatsu, N. Kinoshita, T. Akita, T. Ishida, M. Haruta, *Appl. Cat. A: Gen.*, **2009**, *369*, 8-14.

[26] Y. Önal, *J. Catal.*, **2004**, *223*, 122-133.

[27] S. Biella, L. Prati, M. Rossi, *J. Catal.*, **2002**, *206*, 242-247.

[28] C. Fischer, M. Adam, A. C. Mueller, E. Sperling, M. Wustmann, K.-H. van Pée, S. Kaskel, E. Brunner, *ACS Omega*, **2016**, *1*, 1253-1261.

[29] T. Ishida, N. Kinoshita, H. Okatsu, T. Akita, T. Takei, M. Haruta, *Angew. Chem. Int. Ed.*, **2008**, *47*, 9265-9268.

[30] A. M. Cañete-Rodríguez, I. M. Santos-Dueñas, J. E. Jiménez-Hornero, A. Ehrenreich, W. Liebl, I. García-García, *Process Biochem.*, **2016**, *51*, 1891-1903.

[31] O. V. Singh, R. Kumar, *Appl. Microbiol. Biotechnol.*, **2007**, *75*, 713-722.

[32] P. Beltrame, M. Comotti, C. D. Pina, M. Rossi, *J. Catal.*, **2004**, *228*, 282-287.

[33] P. Beltrame, M. Comotti, C. Della Pina, M. Rossi, *Appl. Cat. A: Gen.*, **2006**, *297*, 1-7.

[34] T. Benkó, A. Beck, O. Geszti, R. Katona, A. Tungler, K. Frey, L. Guczi, Z. Schay, *Appl. Cat. A: Gen.*, **2010**, *388*, 31-36.

[35] C. Baatz, N. Thielecke, U. Prüße, *Appl. Catal. B: Environ.*, **2007**, *70*, 653-660.

[36] C. L. Bianchi, S. Biella, A. Gervasini, L. Prati, M. Rossi, *Catal. Lett.*, **2003**, *85*, 91-96.

[37] T. Ishida, K. Kuroda, N. Kinoshita, W. Minagawa, M. Haruta, *J. Colloid Interface Sci.*, **2008**, *323*, 105-111.

[38] A. Mirescu, H. Berndt, A. Martin, U. Prüße, *Appl. Cat. A: Gen.*, **2007**, *317*, 204-209.

[39] I. Salame, T. J. Bandosz, *J. Colloid Interface Sci.,* **1999**, *210*, 367-374.

[40] N. Dimitratos, J. A. Lopez-Sanchez, G. J. Hutchings, *Chem. Sci.* **2012**, *3*, 20-44.

[41] B. G. Donoeva, D. S. Ovoshchnikov, V. B. Golovko, *ACS Catal.* **2013**, *3*, 2986-2991.